Inorganic Chemistry

ARTICLE

pubs.acs.org/IC

On the Origin of the Relative Stability of Wells−Dawson Isomers: A DFT Study of α-, β-, γ-, α*-, β*-, and γ*-$[(PO_4)_2W_{18}O_{54}]^{6-}$ Anions

Fu-Qiang Zhang,[†] Wei Guan,[‡] Li-Kan Yan,[‡] Yin-Tang Zhang,[†] Mao-Tian Xu,*[,†] Ebenezer Hayfron-Benjamin,[†] and Zhong-Min Su*[,‡]

[†]Department of Chemistry, Shangqiu Normal University, Shangqiu 476000, People's Republic of China

[‡]Institute of Functional Material Chemistry, Department of Chemistry, Northeast Normal University, Changchun 130024, People's Republic of China

Supporting Information

ABSTRACT: Density functional theory calculations have been carried out to investigate α-, β-, γ-, α*-, β*-, and γ*-$[(PO_4)_2W_{18}O_{54}]^{6-}$ Wells−Dawson isomers, which exhibited stability in the order of α > β > γ > γ* > β* > α*, reproduced the experimental observations (α > β > γ), and confirmed the hypothesis of Contant and Thouvenot (γ* > β* > α*). Energy decomposition analysis reveals that both the spatial arrangement of the host $W_{18}O_{54}$ cage (eclipsed or staggered) and its structural distortion induced by the encapsulated guest anions are two dominant factors in control of the stability order, while the influences of host−guest interaction and distortion of the guest anions are very small. A building block decomposition approach is designed and provides an effective means to clarify the detailed relationship between the local distortion and energy. By using this method, it is found that the eclipsed belt, and in particular the staggered belt, significantly distort the two caps inside the Wells−Dawson structure. Notably, there is a direct relationship between the overall stability and distortion in the belts, which is proven to be partly originating from the dominance in the quantity of the belt building blocks over that of the caps (12:6). Besides, half-unit $\{XW_9\}$ decomposition confirms that $[(XO_4)_2W_{18}O_{54}]^{n-}$ (X = Si, Ge, Al, and Ga) are thermodynamically instable because of the notable electrostatic repulsion between two $\{XW_9\}$ units induced by the highly charged guest anions.

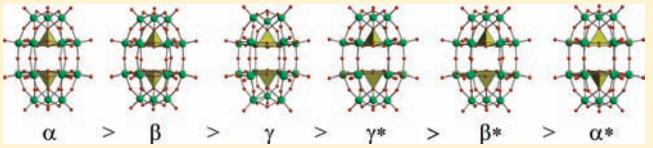

INTRODUCTION

Polyoxometalates (POMs) are molecular metal−oxide clusters characterized by a vast structural diversity and have captured the attention of scientists from many fields such as catalysis, biology, medicine, and materials science.[1] Besides the best-known Keggin anions,[2] a notable subset of POMs are those of the classic Wells−Dawson (WD) structures incorporating two tetrahedral guest anions, $[(XO_4)_2M_{18}O_{54}]^{n-}$ (M = Mo, W, V; X = Cl,[3] S,[4] P,[5] As,[6] V,[7] etc.), which were initially isolated by Wu,[8] structurally postulated by Wells,[9] and determined by Dawson,[10] and, since then, the subject of a vast number of studies.[11] In 1970, Baker and Figgis[12] predicted the existence of six possible isomers formally named α, β, γ, α*, β*, and γ*,[13] differing in the relative orientations of the trinuclear $\{M_3O_{13}\}$ caps or half $\{XW_9\}$ units. However, only four kinds, including the α, β, γ, and γ* isomers, have actually been observed.[14,15]

The dominant isomerism in the WD structure, which involves the $\{M_3O_{13}\}$ cap, has been observed in many structural families of POMs and approximately those in close-packed metal−oxide domains occurring on the steps and corners of reactive metal−oxide surfaces,[1] and it is strongly desired to clarify such a common phenomenon in the POM field. For many years, the structural rearrangement from the β-WD isomer to the more symmetric α one has been observed[16] and only recently has the relative α/β stability been established by Hill and Anderson[17] via the kinetics and thermodynamics equilibrium of α/β-$[P_2W_{18}O_{62}]^{6-}$ (4.4 ± 0.6 and 3.8 ± 0.6 kcal/mol in the solid state and solution, respectively). Poblet and co-workers[18,19] theoretically investigated the small energy difference between α- and β-$[P_2M_{18}O_{62}]^{6-}$ (M = Mo and W) isomers, and they attributed the greater intrinsic stability of the α structure to its favorable metal−oxygen $M_{18}O_{54}$ cage. Contant, Thouvenot, and co-workers[13] have made important contributions in this research field; e.g., on the basis of the new synthesized WD structures, they systematically studied the known WD isomeric types including the isomerization path (γ → β → α) and the enhanced oxidizing power (α < β < γ) of $[X_2W_{18}O_{62}]^{6-}$ (X = P and As). In their studies, these authors also suggested that there is a large amount of tension inside the WD belt region, classified the six isomers into staggered-belt (α*, β*, and γ*) and eclipsed-belt (α, β, and γ) groups, and further predicted that the former ones are always less stable than the latter (α* < β* < γ* < γ < β < α). In particular, the new fast-emerging family of nonconventional WD anions incorporating nontetrahedral anions (such as single-pyramidal XO_3,[20] two-pyramidal SO_3,[21] trigonal-prismatic XO_6,[22] ditetrahedral P_2O_7,[23] and hexafluorosodate NaF_6[24])

Received: January 29, 2011
Published: April 28, 2011

enhances the complexity of the cap-rotational isomerism. For instance, Cronin, Long, and co-workers[22a] recently obtained the peculiar $[H_4W_{19}O_{62}]^{6-}$ species hosting a trigonal-prismatic WO_6^{6-} subunit, and by means of density functional theory (DFT) calculations, they showed that the γ isomer is the most stable arrangement ($\gamma > \alpha > \beta$), which quite differs from the well-known $\alpha < \beta < \gamma$ of classic WD anions.

We have endeavored to clarify the isomerism in POMs based on the topology and DFT method,[25] with the basic objective of a deep understanding of such a common phenomenon as well as their closely related properties. Herein, the relative stability of WD isomers has first been analyzed by using energy decomposition as well as building-block analysis. The selection of six WD $[P_2W_{18}O_{62}]^{6-}$ isomers is due to the following several reasons:[17] (i) the classic WD is the most typical representative of dominant isomerism involving cap or half-unit rotation accompanied by very slight structure and property differences and thus provides a very good opportunity and challenge for theoretical studies; (ii) $[P_2W_{18}O_{62}]^{6-}$ is one of the best-known and most-studied species in POMs from 1920,[26] and besides many synthetic and structural studies on these isomers, detailed thermodynamic and kinetic information of α/β are available; (iii) finally, the polyoxotungstates have been proven to have higher symmetries than the corresponding spiral polyoxomolybdates,[27] and the selection of $[P_2W_{18}O_{62}]^{6-}$ rather than $[P_2Mo_{18}O_{62}]^{6-}$ significantly reduces the computational demands.

COMPUTATIONAL DETAILS

All of the calculations were performed at the DFT level by using the *ADF2008.01* suite of programs.[28] The exchange and correlation energies were calculated using the recent Keal and Tozer density functionals (KT2)[29] within the framework of the generalized gradient approximation (GGA). The basis functions to describe the valence electrons of each atom were triple-ξ plus polarization Slater basis sets (TZP), and the core electrons (O, 1s; P, 1s2p; W, 1s4d) were kept frozen and described by means of single Slater functions. The zero-order regular approximation (ZORA)[30] was adopted in all of the calculations to account for the scalar relativistic effect. Full geometry optimizations were carried out on each structure in the presence of the conductor-like screening solvent model (COSMO[31]) with a solute dielectric constant of 78.4 (water). The ionic radii for the POM atoms, which actually define the cavity in the COSMO, are 1.72, 1.85, and 1.992 Å for O, P, and W, respectively. The value of the numerical integration parameter used to determine the precision of numerical integrals was 5.5. Spin-unrestricted calculations were performed for all of the open-shell systems. Frequency analyses are also implemented on the six optimized $[P_2W_{18}O_{62}]^{6-}$ to make sure that they are indeed stable structures. The short-hand notation for the WD anion without O atoms, charge, and brackets is used, e.g., P_2W_{18} for $[P_2W_{18}O_{62}]^{6-}$ and $P_2W_{18}1e$ for $[P_2W_{18}O_{62}]^{7-}$, where e specifies the number of the blue electrons.

RESULTS AND DISCUSSION

Structure. Among the six Baker–Figgis[12] WD anions, the α, β^*, and γ structures all form D_{3h}-symmetric $M_{18}O_{54}$ (M = Mo, W, V, etc.) cages, while the α^*, β, and γ^* analogues form D_{3d}-symmetric $M_{18}O_{54}$ ones, and, on the other hand, the α, β, and γ structures all encapsulate two eclipsed (D_{3h}) anions (XO_4^{n-}), while the α^*, β^*, and γ^* species incorporate two staggered (D_{3d}) ones.[13] Consequently, the α and γ clusters ideally adopt D_{3h} symmetry, whereas α^* and γ^* take up D_{3d} symmetry; however, the mismatch of the outer cage and the inner tetrahedral anions reduces the symmetries of both the β and β^* structures to C_{3v}.

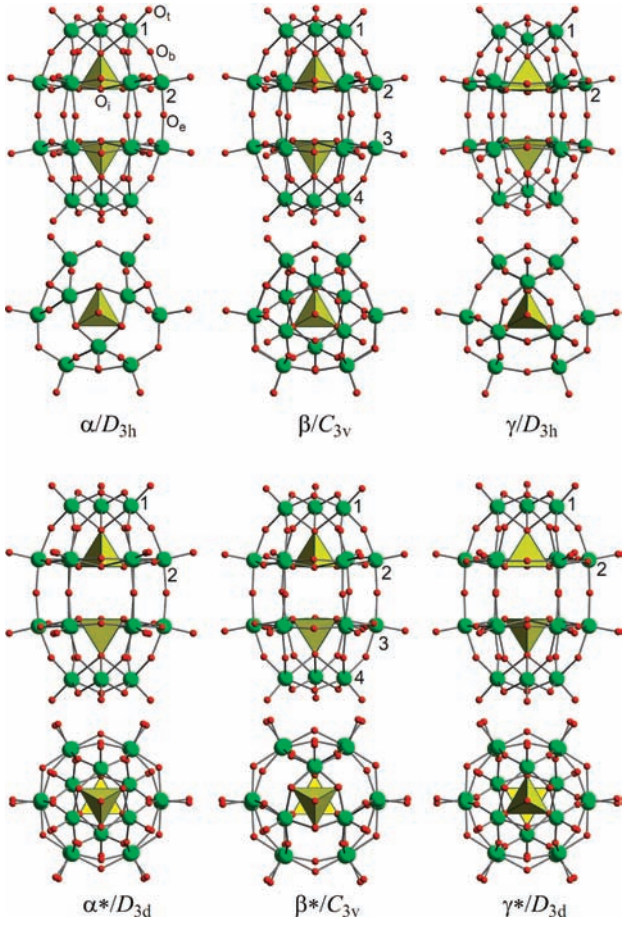

Figure 1. Ball-and-stick representations (top and side views) of the α-, β-, γ-, α^*-, β^*-, and γ^*-$[(PO_4)_2W_{18}O_{54}]^{6-}$ isomers. Four types of O atoms are given: terminal (O_t), interior (O_i), bridging (O_b), and equatorial (O_e). The numbers denote different kinds of octahedral building units in the structure.

Indeed, in our calculations, all of the six P_2W_{18} isomers respectively favor their ideal symmetries (α/D_{3h}, β/C_{3v}, γ/D_{3h}, α^*/D_{3d}, β^*/C_{3v}, and γ^*/D_{3d}), confirming the more recent work of Poblet and co-workers.[27] The obtained structures are shown in Figure 1, and the important parameters are provided in Table 1. As can be seen, the inclusion of the solvent effect significantly improves the calculated structures;[32] e.g., besides nonbonding distances including the P–P distance between two encapsulated anions, the previously difficult parameters such as the bond length of W–O_t[18] (calculated as 1.721–1.722 Å vs averaged 1.710 Å in the experiment;[5d] O_t denotes a terminal oxo ligand as labeled in Figure 1) and the linear angles of equatorial W–O_e–W linking two belts (179.4° vs averaged 179.0° in the experiment;[5d] O_e denotes equatorial oxo ligands) are all well reproduced. The largest deviation is ~0.02 Å observed in the P–O_i (O_i denotes the interior oxygen ligand) bond length, and this validates the employed computational method nicely.

The P_2W_{18} structure can be viewed as an assembly of two kinds of $\{PW_9\}$ half-units (A-α-PW_9 and A-β-PW_9; Figure 1),[33] and inside the two hexagonal belts, the distance between neighboring octahedra (W_b–W_b) exhibits alternative short and long separation under the influence of the interior PO_4^{3-} (Figure S1 in the Supporting Information).[13] In the assembly of the α, β, or γ structure, the hexagonal belts of two $\{PW_9\}$ halves are arranged in an eclipsed

dx.doi.org/10.1021/ic200203s |*Inorg. Chem.* 2011, 50, 4967–4977

Table 1. Optimized Distances[a] (Å) and LUMO Energies of the Six $[(PO_4)_2W_{18}O_{54}]^{6-}$ Isomers

anion	P−O_i	W−O_i	W−O_t	W−O_b	P−P	W−O_e−W[b]	LUMO (eV)[c]
α/D_{3h}	1.544−1.589	2.345−2.355	1.721−1.722	1.895−1.921	3.981	161.2	−4.19 (−6.46)
expt[d]	1.531−1.569	2.306−2.408	1.679−1.743	1.863−1.940	3.986	159.7−163.4	
β/C_{3v}	1.545−1.592	2.352−2.362	1.721	1.894−1.924	3.975	165.1	−4.24 (−6.52)
γ/D_{3h}	1.547−1.592	2.362−2.369	1.721	1.888−1.924	3.986	171.3	−4.31 (−6.57)
α^*/D_{3d}	1.547−1.598	2.355−2.388	1.721−1.722	1.884−1.921	3.915	171.5	−4.28 (−6.50)
β^*/C_{3v}	1.545−1.594	2.354−2.388	1.721	1.887−1.920	3.955	169.5	−4.24 (−6.51)
γ^*/D_{3d}	1.547−1.591	2.377−2.685	1.721	1.884−1.923	3.972	177.0	−4.23 (−6.55)

[a] Observed intervals are given. [b] Equatorial W−O−W angle linking two belts. [c] LUMO energies of the host cage are in parentheses. [d] X-ray data of α-$[(PO_4)_2W_{18}O_{54}]^{6-}$ from ref 5d.

pattern (eclipsed belt) along the direction of the principal C_3 axis and the nonbonding alternation is naturally maintained, as shown by W_b−W_b differences inside the same belt (0.331−0.399 Å[34]) and a very small upper/below W_b−W_b deviation (0.00−0.035 Å[35]) between the two belts. Conversely, in the building of the α*, β*, or γ* framework, the hexagonal belts of both halves are arranged in staggered style (staggered belt). As a result, for better mutual adaptation with respect to their common edges, the reverse rearrangements (distortion) are required for both halves to reduce such an alternation feature, as evidenced by the decreased W_b−W_b differences (0.251−0.334 Å[36]) and large upper/below W_b−W_b deviation (0.251−0.334[37]) between the two belts. Notice that the α*, β*, and γ* isomers can be derived formally from the 60° rotation of one overall $\{XW_9\}$ unit from the α, β, and γ isomers (α → α*, β → β*, and γ → γ*), respectively, and a comparison of the W_b−W_b separation between the three pairs of half-unit-rotation isomers thus provides more direct proof, e.g., α (0.345 Å) > α* (0.251 Å), β (0.365 Å) > β* (0.293 Å),[38] and γ (0.382 Å) > γ* (0.334 Å). Also, the order of 0.094 Å (α → α*) > 0.072 Å (β → β*) > 0.048 Å (γ → γ*) clearly shows that α* and γ* have the largest and least structural arrangements, respectively. In these cases, the large rearrangement denotes a pronounced distortion in the structure (α* > β* > γ*), in accordance with the calculated distortion energy (α* < β* < γ*), as discussed in detail later.

Specifically, each hexagonal belt is composed of six equivalent corner-sharing $\{MO_6\}$ octahedra, in which the six metal sites are strictly coplanar whereas the six bridging O atoms constitute a chair conformation.[39] Noting the tension among octahedra partly located at the joint corners, it is not surprising to find that the six bridging O atoms adopt the most favorable configuration, fully resembling the six classical C sp^3 atoms in the most stable cyclohexane. Furthermore, the decrease in the chair arrangement with an order of α > β > γ (torsion angle of the O atoms in the M_6O_6 circle, 36.2°, 32.4°/21.8°, and 13.4° for α, β, and γ, respectively) implies torsion enhancement and reduced stability, in well agreement with the experimental observation (α > β > γ[13,40]). As expected, rotation from the eclipsed-belt structures to the staggered-belt ones is always accompanied by a significant decrease in the chair conformation, i.e., α → α* (25.1°) > β → β* (10.6°/7.0°) ∼ γ → γ* (10.0°),[41] generally in common with the changes observed in W_b−W_b alternation separations. It is noted that Contant and Thouvenot[13] first emphasized the difference between the WD structures with staggered and eclipsed belts. They observed that, inside the eclipsed-belt α-X_2W_{18} (X = P, As), the equatorial O−O alternation linking the halves (middle) is reversed to that linking the belt and cap (upper), whereas this feature is absent in the case of the staggered-belt γ*-$[X_2W_{18}O_{62}]^{6-}$.[11j]

Table 2. Relative Energies (kcal/mol)[a] of the Six $[(PO_4)_2W_{18}O_{54}]^{6-}$ Isomers at the GGA-KT2/TZP Level

anion	ΔG	ΔE_t[b]	ΔFIE	ΔE_{free}	ΔDE (ΔDE_{guest}/ΔDE_{host})	ΔE_{host}
α/D_{3h}	0.0	0.0 (0.0)	0.0	0.0	0.0 (0.0/0.0)	0.0
β/C_{3v}	−4.8	−5.1 (−6.1)	−0.6	−3.9	−0.5 (0.7/−1.2)	−4.5
γ/D_{3h}	−6.8	−6.3 (−8.8)	0.5	0.0	−6.8 (1.1/−7.9)	−6.8
α^*/D_{3d}	−22.7	−23.6 (−25.5)	−0.1	−3.9	−19.6 (0.9/−20.4)	23.5
β^*/C_{3v}	−12.8	−13.6 (−16.0)	0.7	0.0	−14.3 (0.6/−14.9)	−14.3
γ^*/D_{3d}	−9.5	−9.4 (−13.1)	1.6	−3.9	−7.0 (0.9/−7.9)	−11.0

[a] Defined as the single-point energy of α minus that of the others in the gas phase, and negative values denote disfavored energies. [b] Data in parentheses are obtained within inclusion of COSMO.

Actually, this behavior is general and can be found in all of the eclipsed/staggered-belt pairs (i.e., α/α*, β/β*, and γ/γ*; Figure S2 in the Supporting Information). One slight exception is that, inside the β* structure, equatorial O−O alternation is still observed because it owns nonequivalent halves.

Alternatively, the WD structure can be viewed as an assembly of the one double-layer hexagonal cylinder capped with two polar $\{W_3\}$ triads,[42] and the size of such ellipsoidal structures can be simply characterized by two kinds of metal−metal distances, i.e., W_p−W_p between two poles[43] and W_b−W_b between two opposite sites within the same hexagonal belt. In the case of eclipsed-belt structures, both W_p−W_p (9.815, 9.836, and 9.868 Å for α, β, and γ, respectively) and W_b−W_b (7.010, 7.024,[44] and 7.046 Å for α, β, and γ, respectively) increase slightly with the trend of α < β < γ, demonstrating that the size of the anions expanded substantially in both the polar and radial directions with very similar scale (0.035−0.047 Å). This behavior can be further verified by the O−O distances between corresponding terminal O atoms owned by the metal ions, e.g., polar 12.165/α < 12.176/β < 12.242/γ Å[45] and radial 10.339/α < 10.342/β[46] < 10.365/γ Å, respectively. However, the size of the cap remains fairly constant, as exhibited by the slightly varied W_c−W_c distance (∼0.01 Å, 3.361−3.373 Å[47]) inside the $\{W_3\}$ triad. In contrast, the three staggered-belt counterparts (α*, β*, and γ*) having very similar axial sizes (W_p−W_p of 9.804/9.815, 9.839/9.836, and 9.872/9.868 Å for α*/α, β*/β, and γ*/γ, respectively) are somewhat fat (W_b−W_b, 7.041−7.085 Å). Particularly, there is a substantial increase in W_c−W_c (3.347/α* < 3.385/β*[48] < 3.395/γ* Å), and this reflects that the poles turn to taper in the order of γ* < β* < α*. As a result, among the six isomeric structures, α* and γ* have the most spiky and most flat caps, respectively.

dx.doi.org/10.1021/ic200203s |Inorg. Chem. 2011, 50, 4967–4977

Relative Stabilities. Our calculations show that the stability gradually decreases with order of α > β > γ > γ* > β* > α* (Δ*G* and ΔE_t in Table 2). For the eclipsed-belt structures, the well-known α structure (αα*E*[33]) assembled from two eclipsed A-α-PW_9 half-units is the most stable out of the six isomers. Formal 60° rotation of one or both of the polar {W_3O_{13}} caps would generate β (composed of A-α-PW_9 and A-β-PW_9 units, α*βE*) and γ isomers (composed of two A-β-PW_9 units, *ββE*), respectively, accompanied by 4.8 and 6.8 kcal/mol increases in the Gibbs free energy (Δ*G*). Apparently, besides the stability order of α > β > γ, which agrees well with the experimental observation,[13] the α/β difference (Δ*G*, 4.8 kcal/mol) that we obtained reproduces very well the latest experimental data (3.8 ± 0.6 kcal/mol).[17] In the case of the staggered-belt structures, the α* structure (αα*S*) built from two A-α-PW_9 half-units is the least stable among the six isomers. Rotation of one or both of the polar {W_3O_{13}} caps would generate β* (composed of A-α-PW_9 and A-β-PW_9 units, α*βS*) and γ* isomers (composed of two A-β-PW_9 units, *ββS*), accompanied by 9.9 and 13.2 kcal/mol decreases in energy, respectively. Remarkably, on the one hand, the stability order of α* < β* < γ* fully confirms the hypothesis of Contant and Thouvenot,[13] and, on the other hand, the calculated high energies of α* and β* above the α isomer (22.7 and 12.8 kcal/mol, respectively) clearly demonstrate their thermodynamic instabilities and thereby can be attributed to their absences in experiments to date. Moreover, the electronic contribution to the Gibbs free energy is much larger than the entropic term,[72b] and, consequently, the computed ΔE_t is very close to Δ*G* (Table 2) and is used to discuss the relative stabilities of these POM species in a later section for simplicity.

The WD structure is one of the most representative of the host−guest complexes, in which the inner PO_4^{3-} and the outer $W_{18}O_{54}$ are well separated, as indicated by large W−O_i distances (2.345−2.388 Å) with very small bond order[49] (0.17−0.23; Table S1 in the Supporting Information). As a result, the six WD structures can be viewed as being assembled by the trapping of two charged PO_4^{3-} guest molecules in the neutral $W_{18}O_{54}$ host and reformulated as $2PO_4^{3-}@W_{18}O_{54}$ (the clathrate model[50]). Many studies have shown that it is a sound model for POMs,[19,51] and on that basis, the electronic energy of each P_2W_{18} can be decomposed as follows:

$$2PO_4^{3-}(\text{free}) + W_{18}O_{54}(\text{free}) \rightarrow 2PO_4^{3-}@W_{18}O_{54} \quad (1)$$

Also, the energy differences with respect to the six isomeric anions can be evaluated using

$$\Delta E_t = \Delta E_{free} + \Delta DE(\Delta DE_{guest} + \Delta DE_{host}) + \Delta FIE \quad (2)$$

where E_t represents the energy of the optimized WD anion, E_{free} denotes the sum of energies of the fully relaxed $W_{18}O_{54}$ (E_{host}) and two PO_4^{3-} (E_{guest}), DE is the sum of the deformation energies of $W_{18}O_{54}$ and two PO_4^{3-} from their fully relaxed conformations (DE_{host} + DE_{guest}), and FIE represents the host−guest interaction between $W_{18}O_{54}$ and two PO_4^{3-}. The prefix "Δ" denotes the energy difference between β, γ, α*, β*, and γ* and the reference α structure. To facilitate systematic comparisons, all of the data used here are single-point energies in the gas phase of the associated structures optimized in the solvent phase. Table 2 lists all of the important data, where a negative value denotes a disfavored energy. Several points can be drawn from these values. (1) The energy difference in the host (ΔE_{free}, −3.9 kcal/mol) is the principal factor governing the relative stability (ΔE_t). Notice all six isomeric structures sharing the same guest PO_4^{3-} anion, and ΔE_{free} thus reflects the intrinsic superiority of the eclipsed $W_{18}O_{54}$ cage (D_{3h}) over the staggered one (D_{3d}) in the spatial arrangement, i.e., α, β*, and γ are more favorable in cages than the other three (α*, β, and γ*). For instance, the promoted stabilities of α over β (α > β) and γ over γ* (γ > γ*) are primarily stemming from this fundamental origin (78.2% and 74.8%[52]), while that of β* over α* (β* > α*) is also 39.5% coming from this term (ΔE_{free}). (2) The influence of the host−guest interaction (ΔFIE) is minor. Despite the very large absolute data (FIE, −807.0 to −809.2 kcal/mol; Table S3 in the Supporting Information) that may account for the assembly of the host−guest structures,[53] all of ΔFIE are calculated as very small (−0.6 to −1.6 kcal/mol) and contribute slightly to ΔE_t (<13%[54]), reflecting the intrinsic similarity of the six isomeric structures in host−guest interaction. (3) The different deformation degrees in the structure (ΔDE) are another important factor. DE is composed of two components, the guest (DE_{guest}) and host (DE_{host}). As expected, the distortions observed in all guest PO_4^{3-} molecules are small (DE_{guest}, 3.1−3.7 kcal/mol), and their subtle energy differences (ΔE_{guest}, <1.1 kcal/mol) are completely in line with the slight structural differences (P−O_i with ranges of polar 1.534−1.547 Å and radial 1.589−1.598 Å; P−O−P angles with ranges of axial 107.6−107.9° and radial 111.0−111.3°).[55] By contrast, distortion in the $W_{18}O_{54}$ cage (DE_{host}, 114.2−134.7 kcal/mol) is very large and that constitutes the major part of the distortion of the overall structure (DE). As shown in Figure 2, the consistently decreased ΔDE_{host} displays that distortion of the host cage is enhanced with the order of α < β < γ < γ* < β* < α*, which coincides with variations of the structural parameters as mentioned previously and validates Contant and Thouvenot's assumption[13] of larger distortions in the staggered-belt structures than in the eclipsed-belt counterparts. For instance, the smaller distortions in the β and γ* cages are completely (100%) answered for the enhanced stability of β over γ (β > γ) and γ* over β* (γ* > β*), despite their disfavored D_{3d} cage in the arrangement; while the promoted stability of β* over α* (β* > α*) is also ∼53% from the small ΔDE_{host} of β*, besides its superiority in the D_{3h} cage. Moreover, among all of the components of ΔE_t, only the contribution of ΔDE_{host} is always negative, revealing that it is the exclusive reason undermining the stability of the isomers. Briefly, the spatial arrangement of the host cage and its distortion are two principal factors that control the relative stabilities of the WD isomers, whereas the influences of the host−guest interaction and the guest distortion are always small. This result is reminiscent of the α/β-Keggin relative stability with low charge.[25b,56] It is noteworthy that the magnitudes of host distortion (DE_{host}) and host−guest interaction (FIE) depend strongly on the charge of the guest molecules, e.g., generally preserved in the isocharged $[(AsO_4)_2W_{18}O_{54}]^{6-}$ (114.1−135.9/DE_{host}, −776.3 to −784.5/FIE kcal/mol, respectively; Table S9 in the Supporting Information) but dramatically reduced in lowly charged $[(SO_4)_2W_{18}O_{54}]^{4-}$ (50.0−62.5/DE_{host}, −477.1 to −480.8/FIE kcal/mol, respectively; Table S12 in the Supporting Information). However, the patterns of ΔDE_{host}, ΔDE_{guest}, ΔDE, and ΔFIE observed in PW_{18} are generally maintained in these structures and thus result in the same stability order (α > β > γ > γ* > β* > α*; Figures S3 and S4 in the Supporting Information).

In fact, the formula (2) can be transformed to

$$\Delta E_t = \Delta E_{host}(\Delta E_{free} + \Delta DE_{host}) + \Delta DE_{guest} + \Delta FIE \quad (3)$$

dx.doi.org/10.1021/ic200203s |*Inorg. Chem.* 2011, 50, 4967–4977

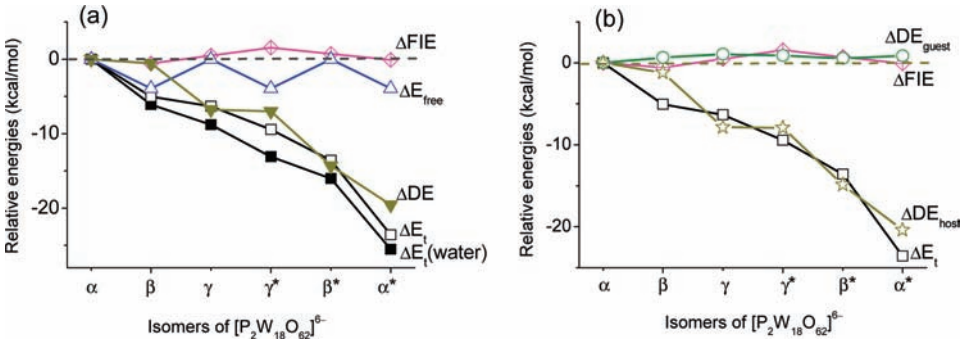

Figure 2. Seven kinds of relative energies as a function of six $[(PO_4)_2W_{18}O_{54}]^{6-}$.

Table 3. Bonding Energies (au) of $O_t{=}W(OH)_4$ for (O−H = 0.9615 Å) for Six $[(PO_4)_2W_{18}O_{54}]^{6-}$ Isomers

isomer	1[a]	2	3	4	average[b]	belt (kcal/mol)[c]	cap (kcal/mol)[c]
α/D_{3h}	−2.42604	−2.41922			−2.42149 (0.0)	0.0	0.0
β/C_{3v}	−2.42630	−2.41826	−2.41798	−2.42923	−2.42134 (0.1)	0.7	−1.1
γ/D_{3h}	−2.42871	−2.41731			−2.42111 (0.2)	1.2	−1.7
α^*/D_{3d}	−2.42724	−2.41393			−2.41835 (2.0)	3.3	−0.8
β^*/C_{3v}	−2.42687	−2.41650	−2.41583	−2.42634	−2.41965 (1.2)	1.9	−0.4
γ^*/D_{3d}	−2.42745	−2.41631			−2.42003 (0.9)	1.8	−0.9

[a] The numbers 1−4 denote the different kinds of building blocks in the structure, as labeled in Figure 1. [b] Relative energies (kcal/mol) in parentheses, where positive values denote disfavored energies. [c] Relative energies on average.

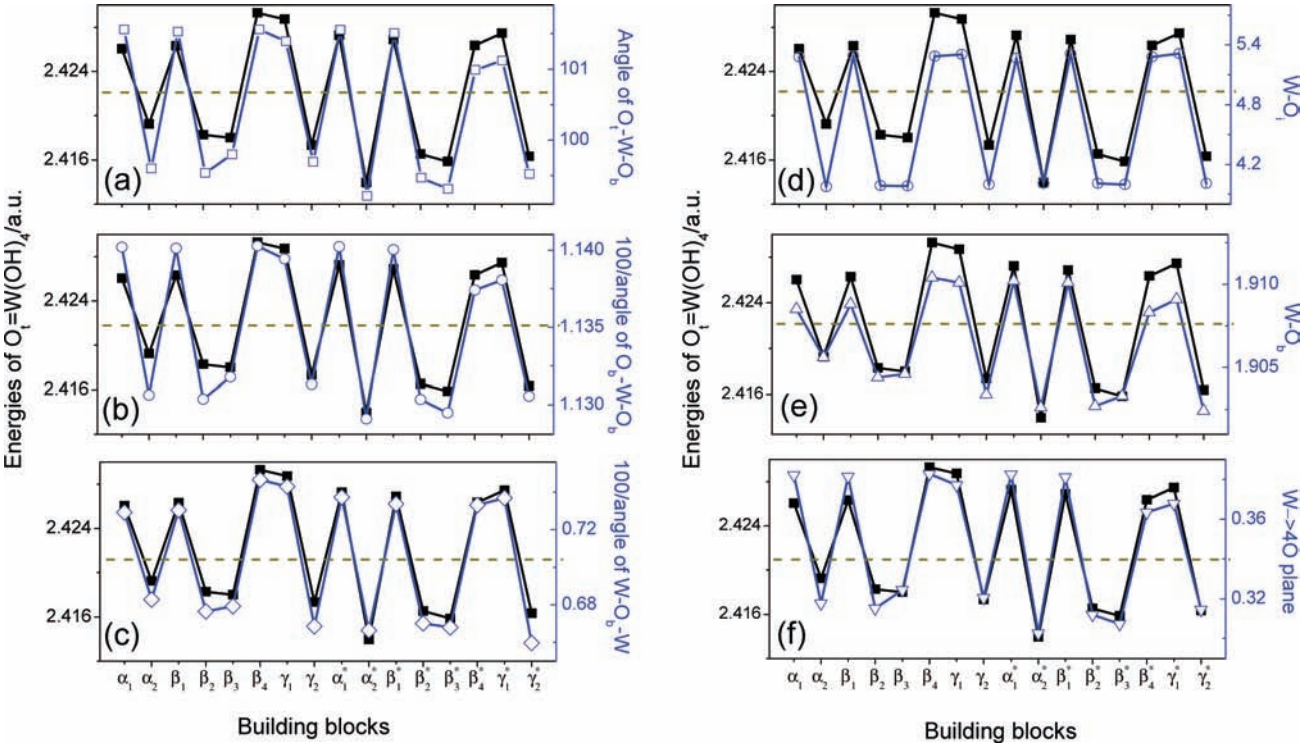

Figure 3. Dependences of $[O_t{=}W(OH)_4]$ energies (au, absolute values) on six kinds of structural parameters. Positive values denote favorable energies.

where ΔE_{host} (the sum of ΔE_{free} and ΔDE_{host}) is the single-point-energy difference of the six host cages that are extracted from the optimized anions. Be aware of the minor contributions of ΔDE_{guest}, ΔFIE, and even the sum of both of them (<12.0%); ΔE_t is therefore dominated by the primary source of ΔE_{host} (>88.0%), as is clearly shown in Figure 2b; namely, the more stable anions always possess a more stable host $W_{18}O_{54}$ cage, and vice versa. Consequently, the relative stabilities of the WD

dx.doi.org/10.1021/ic200203s |Inorg. Chem. 2011, 50, 4967–4977

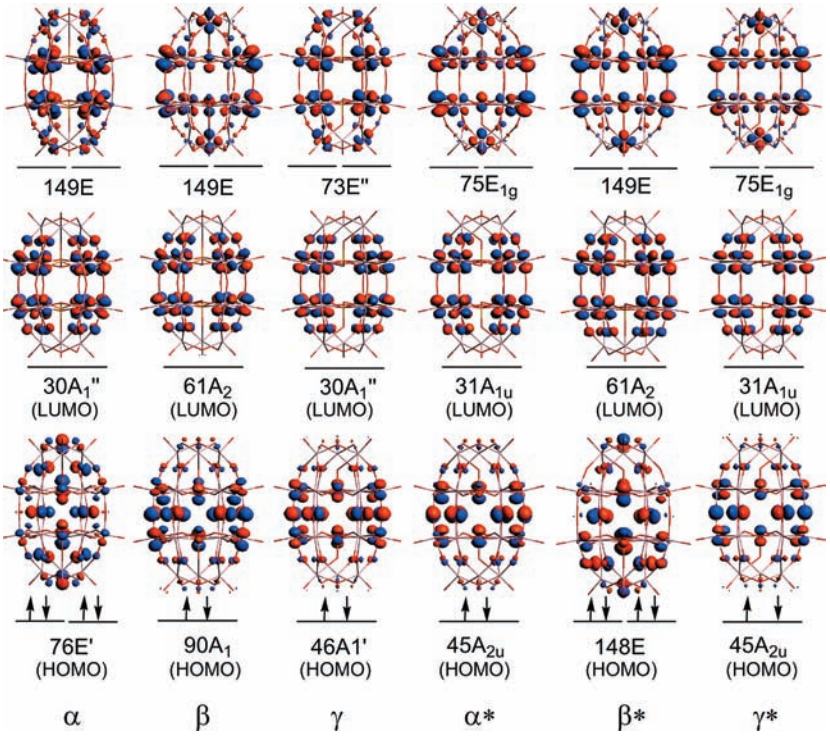

Figure 4. Spatial representation of the frontier molecular orbitals of six $[(PO_4)_2W_{18}O_{54}]^{6-}$.

structures can be simply evaluated by their host cages, in spite of its eclipsed or staggered spatial arrangement. This result sheds new insight into the basic differences among the six WD isomeric structures.

To further characterize the differences of the six $W_{18}O_{54}$, we decompose each cage into 18 pyramidal building blocks, $\{O_t{=}W(OH)_4\}$, in which four H atoms are added along the boundary $O_b{-}W$ (O_b is a bridging oxo ligand) bond with a distance of 0.9615 Å,[57] aimed to simulate the possible chemical environment of the fragment inside the overall structure. Two kinds of blocks are present in the D_{3h}- or D_{3d}-symmetric α/D_{3h}, γ/D_{3h}, α^*/D_{3d}, and γ^*/D_{3d} comprised of two equivalent $\{PW_9\}$, and four kinds are observed in the C_{3v}-symmetric β or β^* built from nonequivalent halves. By this approach, it is found that the pyramidal units of the $W_{18}O_{54}$ cages are destabilized in the order of $\alpha > \beta > \gamma > \gamma^* > \beta^* > \alpha^*$ (average data in Table 3), reproducing very well the overall trend of ΔE_{host}. Two key points can be drawn from the values in the table.

First, the building blocks of the polar triad are notably more stable than those of the belt with ~6.5 kcal/mol on average. In Figure 3, the peaks representing energetically favored units are all from the polar part, whereas the valleys denoting energetically disfavored units are all from the belt region. This clear distinction discloses the primary characteristics of the ellipsoidal WD framework, within which the polar cap can be taken as a single entity that structurally distinguishes it from the equatorial belt, as evidenced by many experimental facts (e.g., the stable trimetallic $M_3O_{13}^{2-}$,[58] lacunary $P_2W_{15}O_{56}^{12-}$ missing of one polar group,[59] borophosphate anion contains a two-layer $\{W_{12}\}$ belt,[60] etc.), on the one hand, and offers a qualitative explanation of the special stability of the quasi-spherical α-Keggin structure assembled entirely from four "polar" caps, on the other hand (e.g., the geometry rearrangement of the WD to the Keggin structure[61]). More interestingly, the energy of the block unit (E_W) keeps a close relationship with its geometry parameters such as the bond lengths of $W{-}O_b$ and $W{-}O_i$, angles of $W{-}O_b{-}W$, $O_t{-}W{-}O_b$, $O_b{-}W{-}O_b$, etc. As shown in Figure 3, the strong dependencies of E_W on three parameters that are closely related to the pseudooctahedral bonding environment of the metal center, including its direct relationship with the angle of $O_t{-}W{-}O_b$ ($E_W \sim O_t{-}W{-}O_b$; Figure 3a) and the bond length of $W{-}O_i$ ($E_W \sim W{-}O_i$; Figure 3d) and its inverse relationship with the angle of $O_b{-}W{-}O_b$ ($E_W \sim 100/O_b{-}W{-}O_b$; Figure 3b), are combined to suggest that $\{O_t{=}W(OH)_4\}$ is compressed along the axial direction, particularly stronger in the belt than in the cap region (e.g., smaller $O_t{-}W{-}O_b$ of 99.5°/belt vs 101.4°/cap, larger $O_b{-}W{-}O_b$ of 88.5°/belt vs 87.8°/cap, and larger $W{-}O_i$ of 3.99/belt vs 5.29/cap Å, on average). This primary structural feature can be validated straightforward by examining the distance from the W to the four-O_b base plane ($W \rightarrow 4O_b$[62]), e.g., the short 0.314/belt vs long 0.377/cap Å as well as its direct proportion with E_W ($E_W \sim W{-}O_i$; Figure 3f). Correlatively, this kind of distortion will result in large bond angles between building units, e.g., the inverse relationship of $W{-}O_b{-}W$ with E_W ($E_W \sim 100/W{-}O_b{-}W$; Figure 3c) as well as those nearly linear bond angles linking halves (161.2−177.0°), which significantly deviate from the general O sp^4 hybridization[63] and invariably intensify the distortion. The bond length of $W{-}O_b$, despite its very small variation (1.903−1.910 Å), still has a direct relationship with E_W ($E_W \sim W{-}O_b$, Figure 3e), originating from its W d−O p π nature of POMs.[51]

Second, the building unit of the staggered belt is always less favored than that of the eclipsed one with ~1.7 kcal/mol on average. As listed in Table 3, the belt region is destabilized in the order of $\alpha/0.0 < \beta/0.7 < \gamma/1.2 < \gamma^*/1.8 < \beta^*/1.9 < \alpha^*/3.3$ kcal/mol. The data fully confirm the hypothesis of Contant and

dx.doi.org/10.1021/ic200203s |Inorg. Chem. 2011, 50, 4967–4977

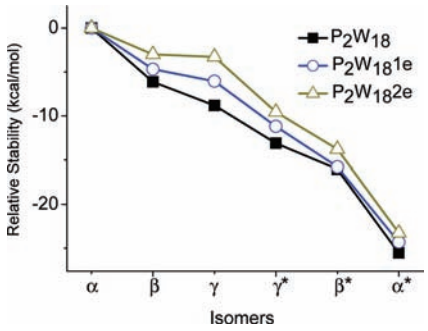

Figure 5. Relative stability (kcal/mol) of oxidized and single- and double-reduced $[(PO_4)_2W_{18}O_{54}]^{6-}$ isomers.

Thouvenot,[13] who predicted a significant structural distortion in the staggered belt over the eclipsed one. It is noteworthy that, in the absence of the guest anion, the alternation in half a $\{W_9\}$[64] bowl is very small (0.015 Å). Consequently, the larger the alternation in the eclipsed belt of the $\{PW_9\}$ anion, the larger the distortion in the structure after PO_4^{3-} is encapsulated, thereby providing a qualitative explanation of the increased W−W alternation order of $\alpha < \beta < \gamma$ (0.345 < 0.365 < 0.382 Å, on average), in accordance with their relative stability ($\alpha > \beta > \gamma$). After a 60° rotation to yield the staggered-belt structures ($\alpha \rightarrow \alpha^*$, $\beta \rightarrow \beta^*$, and $\gamma \rightarrow \gamma^*$), the changes observed in the reduced W−W alternation actually reflect the extra distortions accompanied, e.g., $\gamma^* > \beta^* > \alpha^*$ (0.048 < 0.064 < 0.094 Å on average), in agreement with the energy variations of $\gamma^* < \beta^* < \alpha^*$.

An attractive feature of the structural decomposition approach is the approximate additivity of an individual building-unit energy (E_W), providing access to clarifying the origin of the relative stabilities of these structures. For instance, for the eclipsed-belt structures, in going from α to γ ($\alpha \rightarrow \beta \rightarrow \gamma$), each rotation consistently stabilizes the units in polar caps (~0.6 kcal/mol) but meanwhile destabilizes the belt components (~0.8 kcal/mol). Despite the relatively large stabilizing effects held by the caps, the overall stability is still steadily reduced ($\alpha > \beta > \gamma$) because of twice the contributions of the belt region over the polar cap to the whole structure (12 vs 6). Differently, in the case of the latter four isomeric structures (γ, γ^*, β^*, and α^*), each rotation steadily destabilizes both the cap and belt regions. Regarding the large contribution of the belt components, the decreased energy is enhanced with the order $\gamma > \gamma^* > \beta^* > \alpha^*$. To sum things up, in all cases the double-layer $\{W_{12}\}$ belt is the key region that is responsible for the relative stability of the overall host cage and thereby controls the corresponding anion, in which its dominance in the building-block quantity over that of the caps plays an important role.

Reduced Structures. In the fully oxidized state, all six isomeric P_2W_{18} have the same simple electronic structure constituted of two well-separated sets of molecular energy levels with a clear HOMO−LUMO gap (2.22−2.48 eV). The low-lying orbitals comprise predominately O p nonbonding bands delocalized over the bridging O atoms, while the high-lying orbitals represent very weak π-antibonding interactions between the symmetry-adapted metal d_{xy} and bridging O p orbitals delocalized over the d shells of the W atoms. As shown in Figure 4, the cap and belt metals do not participate equally in the lowest unoccupied molecular orbitals; e.g., LUMO and LUMO+1 are mainly centered on the 12 belt W atoms rather than the two caps. As a direct consequence, for all six structures, the reduction should preferentially take place in the belt region. This prediction can be confirmed by studying the spin density of the single-reduced species, e.g., 0.10e of the belt vs 0.01e of the cap. However, in the case of the double-reduced species, the two *blue* electrons are completely paired and thus yield a singlet ground state, in well agreement with the diamagnetic behavior of α- and β-P_2W_{18}2e in the experiment.[65] This result is general and has been found in other kinds of POMs, e.g., the reduced Keggin anion, in which the strong antiferromagnetic coupling between two delocalized electrons is promoted by electron hopping among molecular fragments.[66,67]

Table 4. First and Second Reduction Potentials (V) for the Studied Complexes

isomer	α	β	γ	α*	β*	γ*
first	−0.50 (−0.77[a])	−0.44	−0.38	−0.44	−0.49	−0.41
second	−0.81 (−1.13[a])	−0.74	−0.69	−0.77	−0.73	−0.74

[a] Experimental values obtained from ref 69.

Full geometry optimizations in the presence of COSMO show that both P_2W_{18}1e and P_2W_{18}2e species share the same stability order with their oxidized P_2W_{18} parent ($\alpha > \beta > \gamma > \gamma^* > \beta^* > \alpha^*$; Figure 5). The distribution of *blue* electrons over the host cages permits implementation of the following host−guest energy decomposition approach:

$$2PO_4^{3-}(\text{free}) + W_{18}O_{54}^{m-}(\text{free}) \rightarrow 2PO_4^{3-}@W_{18}O_{54}^{m-} \quad (4)$$

By utilizing the quantitative energy evaluation previously performed on P_2W_{18} (eqs 2 and 3), we observe that the increased charges carried by the host cage have a slight affect on the overall structure including both the interior PO_4^{3-} and the outer host cage, as exhibited by their unperceived geometry changes as well as the constant energies of DE_{guest}, DE_{host}, and DE (Tables S15 and S18 in the Supporting Information). Differently, the host−guest interaction (FIE) is notably reduced (from −807.0 to −809.2, from −478.2 to −481.4, and from −150.7 to −154.9 kcal/mol for P_2W_{18}, P_2W_{18}1e, and P_2W_{18}2e, respectively) and that can be simply attributed to the increased host−guest electrostatic repulsion. However, the origin of the stability order (ΔE_t) obtained from oxidized structures is maintained; i.e., ΔDE_{host}, ΔE_{free}, and the sum of both of them (ΔE_{host}) are dominant, while ΔDE_{guest} and ΔFIE are subordinate (Figures S5 and S6 in the Supporting Information), further validating our previous results. Besides, the inclusion of COSMO in the computations becomes more important because of the increasing charge of the reduced species. Otherwise, energies would not be reliable in the gas phase, e.g., the slight β/γ and α/γ single-point-energy inversion observed in P_2W_{18}1e and P_2W_{18}2e species, respectively (Tables S16 and S19 in the Supporting Information).

Furthermore, the redox properties of the six P_2W_{18} anions can also be rationalized by the latest theoretical method in solution,[68] which requires determination of the free energy associated with the process

$$[(PO_4)_2W_{18}O_{54}]^{n-}(aq) + e^- \xrightarrow{\Delta G} [(PO_4)_2W_{18}O_{54}]^{(n+1)-}(aq) \quad (5)$$

where the term ΔG represents the free energy of the reduction process in solution and can be approximated by the reduction

dx.doi.org/10.1021/ic200203s |*Inorg. Chem.* 2011, 50, 4967–4977

energy of the complex, due to the difficulties in obtaining the frequency calculation in the presence of COSMO. When the Nernst equation $E^\circ = -\Delta G^\circ/nF$ is combined with the reference value −4.60 eV of the saturated calomel electrode, the reduction potentials (E_{RP}) can be predicted. Table 4 summarizes the calculated first and second reduction potentials, and it can be seen that the theoretical predications agree very well with the experimental data[69] available. Apparently, for the eclipsed-belt species, the oxidizing power increases with a trend of $\alpha < \beta < \gamma$, in line with the experimental observations,[13,65] while for the staggered-belt species, large discrepancies are observed between the first and second E_{RP} ($\gamma^* < \alpha^* < \beta^*$ vs $\alpha^* < \beta^* \sim \gamma^*$). However, it should be noticed that γ^* and β share very similar electrochemical properties in both cases ($\alpha < \beta \sim \gamma^* < \gamma$), which has been observed in β-As_2W_{18} and γ^*-As_2W_{18} experimentally.[13]

More recent studies reveal that the redox properties of POMs depend on the molecular energy level of the LUMO (E_{LUMO}) in the oxidized state, which, in turn, relates closely to the charge and size of the guest molecules, besides the size of the overall structure.[70−72] In the present study, the guest anions in all of the structures are virtually identical as aforementioned and they cannot be the principal reason for the reduction potential trend. On the other hand, the LUMO of an oxidized WD structure is symmetry-adapted d_{xy}-like orbitals centered heavily at the belt metal atoms, and the encapsulation of guest anions modifies the nature of the LUMO little but shifts it upward energetically, originating from the electrostatic repulsion produced by an internal negative charge.[71a] Indeed, the E_{LUMO} values of all six isomeric P_2W_{18} anions depend strongly on the E_{LUMO} values of their respective host cages with a constant difference of 2.26−2.27 eV,[73] and both of them are closely related to the reduction potentials (Figure 6), validating the very recent studies of Poblet and co-workers.[71]

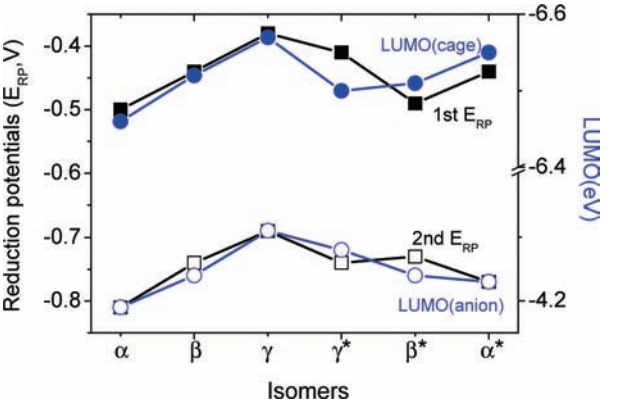

Figure 6. Correlation between the reduction potential (in V) and the LUMO energies (in eV) of anions and host cages.

Formation of $[(XO_4)_2W_{18}O_{56}]^{n-}$ (X = Si, Ge, Al, and Ga) with High Charge. Unlike the Keggin $[(XO_4)M_{12}O_{36}]^{n-}$, which can encapsulate a wide variety of XO_4^{n-} (X = Cl, S, Si, As, Ge, Al, Ga, Fe, Co, etc.), the WD $[(XO_4)_2M_{18}O_{54}]^{n-}$ seems to only accommodate lowly charged anions such as ClO_4^-, SO_4^{2-}, PO_4^{3-}, AsO_4^{3-}, VO_4^{3-}, etc.[3−7] It has been established that the WD structure can be generated by the direct fusion of two half-units, e.g., 2A-α-$[PW_9O_{34}]^{9-}$ → α-$[P_2W_{18}O_{62}]^{6-}$.[74] However, in the cases of $\{XW_9\}$ with X = Si^{IV} and Ge^{IV},[33a] it is assumed that the electrostatic repulsion between the halves induced by the highly charged guest XO_4^{4-} (X = Si, Ge) is so strong that it inhibits the assembly of the overall structure. Also, no conventional but open WD structures are obtained.[75] To clarify such a problem, the interactions between the two $\{XW_9\}$ fragments of the α-$[(XO_4)_2W_{18}O_{54}]^{n-}$ (X = S^{VI}, Se^{VI}, P^V, As^V, Si^{IV}, Ge^{IV}, Al^{III}, and Ga^{III}) series, including four hypothetical structures (X = Si^{IV}, Ge^{IV}, Al^{III}, and Ga^{III}), are estimated based on the bonding energy (E_B) decomposition[76] as

$$E_B = E_P + E_E + E_O \quad (4)$$

where E_P, E_E, and E_O are the Pauli repulsion, electrostatic interaction, and orbital mixing terms, respectively. Among the

Table 5. Relative Bonding Energies (eV) of α-$[(XO_4)_2W_{18}O_{54}]^{n-}$ (X = S, Se, P, As, Si, Ge, Al, and Ga)

isomer	ΔE_P	ΔE_E	ΔE_O	ΔE_B
S	0.00	0.00	0.00	0.00
Se	0.08	0.04	−0.20	−0.07
P	−1.45	−7.13	−0.48	−9.06
As	−1.74	−6.68	−0.53	−8.95
Si	−3.67	−17.37	−0.46	−21.49
Ge	−3.56	−17.10	−0.64	−21.31
Al	−5.67	−28.27	−0.26	−37.07
Ga	−5.57	−28.32	−0.33	−37.00

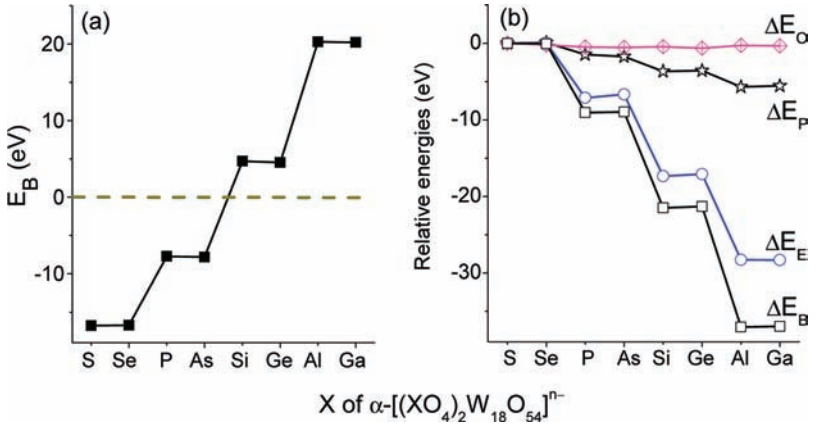

Figure 7. Five kinds of energies as a function of a series of α-$[(XO_4)_2W_{18}O_{54}]^{n-}$ (X = S, Se, P, As, Si, Ge, Al, and Ga).

dx.doi.org/10.1021/ic200203s |Inorg. Chem. 2011, 50, 4967–4977

three components of E_B, the Pauli repulsion[77] acting as the destabilization term is caused by the larger energy shift of the antibonding orbitals to bonding orbitals, whereas E_E and E_O are stabilizing, in which E_E is dominated by the nucleus−electron attractions and E_O arises from the mixing of occupied and unoccupied orbitals.[78] Overall, the total bonding energy (E_B) can be considered a measure of the instantaneous interaction between the two $\{XW_9\}$ fragments inside the WD structure. As can be seen from Table 5, the calculated E_B clearly exhibits its close relationship with the charges of the guest anions (S ∼ Se > P ∼ As > Si ∼ Ge > Al ∼ Ga), in which the least charged α-X_2W_{18} (X = S and Se) are the most favored, while the highest charged α-X_2W_{18} (X = Al and Ga) are the least favored. Notably, there is a clear boundary between the 3− and 4− charged XO_4^{n-}; i.e., at this point, E_B exhibits a qualitative leap from negative to positive (−7.8 to +4.6 eV on average; dashed line in Figure 7a), suggesting that the WD structure accommodating SiO_4^{4-}, GeO_4^{4-}, AlO_4^{5-}, or GaO_4^{5-} is impossible. Further insight can be gained by analysis of the relative energies (the negative value denotes disfavored energy), which takes those of α-S_2W_{18} as the reference. As shown in Figure 7b, the increased charge of the guest molecule does not affect the orbital mixing terms (E_O) but moderately promotes Pauli repulsion (E_p) and significantly enhances electrostatic interaction (E_E). Consequently, E_B is dominated by E_E, which corresponds to the classical electrostatic effects associated with Columbic attraction and repulsion, confirming the key influence that the charges of the guest anions play in the formation of the WD structure.

CONCLUSIONS

In summary, systematic DFT computations have been carried out to investigate the stability of six WD $[(PO_4)_2W_{18}O_{54}]^{6-}$ isomers. In the presence of COSMO, the calculations show that the fully oxidized and single- or double-reduced species share the same stability of α > β > γ > γ* > β* > α* and confirm the hypothesis of Contant and Thouvenot. Several conclusions can be drawn:

(1) Structural parameter analysis shows that the staggered-belt structures, including α*, β*, and γ*, quite differ from the eclipsed-belt structures, such as α, β, and γ isomers, in their distortion scale inside the belt region.

(2) Host−guest energy decomposition clarifies that the relative stabilities of the six isomers mainly stem from their host cages in different arrangements and different distortions induced by the encapsulated guest anions, whereas the influence of the host−guest interaction is slight.

(3) Building-block decomposition reveals that the $\{O_t{=}W(OH)_4\}$ unit of the WD host cage is compressed along the axial direction, particularly more in the belt region than in the cap region.

(4) Calculations performed on the reduced species show that the reduction potential is closely related to the LUMO energy of the oxidized $[(PO_4)_2W_{18}O_{56}]^{6-}$, which, in turn, relies upon the LUMO energy of its host cage.

(5) The half-unit $\{XW_9\}$ fragment energy dissociation confirms the thermodynamical instability of the $[(XO_4)_2W_{18}O_{54}]^{n-}$ (X = Si, Ge, Al, and Ga) species, which originates from the notable electrostatic repulsion induced by the highly charged guest anions of the two $\{XW_9\}$.

This work has broad implications for the understanding of the conventional WD encapsulating other kinds of tetrahedral guest anions, including ClO_4^-, SO_4^{2-}, AsO_4^{3-}, and VO_4^{3-}, which exhibit structural and electronic similarities with the $[(PO_4)_2W_{18}O_{54}]^{6-}$ in this paper. Further studies on these compounds are in progress.

ASSOCIATED CONTENT

Supporting Information. Total bonding energies and relative energies of $[P_2W_{18}O_{62}]^{6/7/8-}$, $[As_2W_{18}O_{62}]^{6-}$, and $[S_2W_{18}O_{62}]^{4-}$ isomers; bonding energies, parameters of the building blocks, Mayer indexes of W−O_i, and alternation of the W−W and O−O distances of six $[P_2W_{18}O_{62}]^{6-}$ isomers, bonding energies (half-decomposition) of $[X_2W_{18}O_{62}]^{n-}$ (X = S, Se, P, As, Si, Ge, Al, and Ga), and seven kinds of relative energies as functions of $[X_2W_{18}O_{62}]^{n-}$ (X = S and As) and $[P_2W_{18}O_{62}]^{6/7/8-}$, respectively. This material is available free of charge via the Internet at http://pubs.acs.org.

AUTHOR INFORMATION

Corresponding Author

*E-mail: xumaotian@sqnc.edu.cn (M.-T.X.), zmsu@nenu.edu.cn (Z.-M.S.). Fax & Tel: +8603702595593.

ACKNOWLEDGMENT

This work is supported by the National Natural Science Foundation of China (Grant 20775047) and the Foundation for Middle-aged and Young Key Teachers of Shangqiu Normal University. We thank Prof. Hai-Shun Wu and Prof. Xian-Ming Zhang for their dedication in discussions of structure distortion.

REFERENCES

(1) (a) Pope, M. T. *Isopoly and Heteropoly Anions*; Springer: Berlin, 1983. (b) Pope, M. T., Müller, A., Eds. *Polyoxometalate Chemistry*; Kluwer Academic: Dordrecht, The Netherlands, 2001. (c) Kozhevnikov, I. V. *Catalysis by Polyoxometalates*; Wiley: Chichester, England, 2002. (d) Hill, C. L.; Prosser-McCartha, C. M. *Coord. Chem. Rev.* **1995**, *143*, 407–455. (e) Mizuno, N.; Misono, M. *Chem. Rev.* **1998**, *98*, 199. (f) Neumann, R. *Prog. Inorg. Chem.* **1998**, *47*, 317–370. (g) Li, G.; Ding, Y.; Wang, J.; Wang, X.; Suo, J. *J. Mol. Catal. A: Chem.* **2007**, *262*, 67–76.

(2) (a) Keggin, J. F. *Nature* **1933**, *131*, 908–909. (b) Keggin, J. F. *Proc. R. Soc. London, Ser. A* **1934**, *144*, 75–100.

(3) (a) Herbstein, F. H.; Marsh, R. E. *Acta Crystallogr.* **1998**, *B54*, 677–686. (b) Zhu, S.; Yue, B.; Shi, X.; Gu, Y.; Liu, J.; Chen, M.; Huang, Y. *J. Chem. Soc., Dalton Trans.* **1993**, 3633–3634.

(4) For example, see: (a) Zhang, J.; Bond, A. M.; Richardt, P. J. S.; Wedd, A. G. *Inorg. Chem.* **2004**, *43*, 8263–8271. (b) Way, D. M.; Cooper, J. B.; Sadek, M.; Vu, T.; Mahon, P. J.; Bond, A. M.; Brownlee, R. T. C.; Wedd, A. G. *Inorg. Chem.* **1997**, *36*, 4227–4233. (c) Neier, R.; Trojanowski, C.; Mattes, R. *J. Chem. Soc., Dalton Trans.* **1995**, 2521–2528. (d) Hori, T.; Tamada, O.; Himeno, S. *J. Chem. Soc., Dalton Trans.* **1989**, *8*, 1491–1947.

(5) (a) D'Amour, H.; Allmann, R. *Naturwissenschaften* **1974**, *61*, 34. (b) Strandberg, R. *Acta Chem. Scand. Ser.* **1975**, *A29*, 350–358. (c) Holscher, M.; Englert, U.; Zibrowius, B.; Holderich, W. *Angew. Chem., Int. Ed.* **1994**, *106*, 2552–2554. (d) Li, Z.; Lin, B.-Z.; Zhang, J.-F.; Geng, F.; Han, G.-H.; Liu, P.-D. *J. Mol. Struct.* **2006**, *783*, 176–183. (e) Vilà-Nadal, L.; Rodríguez-Fortea, A.; Yan, L.-K.; Wilson, E. F.; Cronin, L.; Poblet, J. M. *Angew. Chem., Int. Ed.* **2009**, *48*, 5452–5456.

(6) (a) Lyhamn, L.; Pettersson, L. *Chem. Scr.* **1979**, *12*, 142–152. (b) Ichida, H.; Sasaki, Y. *Acta Crystallogr., Ser. C* **1983**, *39*, 529–532. (c) Wang, J.; Wang, W.; Niu, J. *Inorg. Chem. Commun.* **2007**, *10*, 520.

(7) Liang, D.-D.; Liu, S.-X.; Ren, Y.-H.; Zhang, C.-D.; Xu, L. *Inorg. Chem. Commun.* **2007**, *10*, 933–935.

(8) Wu, H. *J. Biol. Chem.* **1920**, *43*, 189–220.

(9) Wells, A. F. *Structural Inorganic Chemistry*; Clarendon Press: Oxford, U.K., 1945.

(10) Dawson, B. *Acta Crystallogr., Sect. B* **1953**, *6*, 113–126.

(11) For example, see: (a) Constant, R.; Abbessi, M.; Tjpivempt, R.; Hervé, G. *Inorg. Chem.* **2004**, *43*, 3597–3604. (b) Holscher, M.; Englert, U.; Zibrowius, B.; Holderich, W. F. *Angew. Chem., Int. Ed. Engl.* **1994**, *33*, 2491–2493. (c) Keita, B.; Mbomekalle, I. B.; Nadjo, L.; Anderson, T. M.; Hill, C. L. *Inorg. Chem.* **2004**, *43*, 3257–3263. (d) Zhang, J.; Bond, A. M. *Inorg. Chem.* **2004**, *43*, 8263–8271. (e) Anderson, T. M.; Zhang, X.; Hardcastle, K. I.; Hill, C. L. *Inorg. Chem.* **2002**, *41*, 2477–2488. (f) Fang, X.-K.; Anderson, T. M.; Hill, C. L. *Angew. Chem., Int. Ed.* **2005**, *44*, 3540–3544. (g) Bodin, B.; Chen, Y.-G.; Vaissermann, J.; Ruhlmann, L.; Verdaguer, M.; Gouzerh, P. *Angew. Chem., Int. Ed.* **2005**, *44*, 3072–3075. (h) Coronado, E.; Galan-Mascaros, J. R.; Gimenez-Saiz, C.; Gomez-Garcia, C. J.; Laukhin, V. M. *Adv. Mater.* **1996**, *8*, 801–811. (i) Fang, X.-K.; Hill, C. L. *Angew. Chem., Int. Ed.* **2007**, *46*, 3877–3880. (j) Richardt, P. J. S.; Gable, R. W.; Bond, A. M.; Wedd, A. G. *Inorg. Chem.* **2001**, *40*, 703–709.

(12) Baker, L. C. W.; Figgis, J. S. *J. Am. Chem. Soc.* **1970**, *92*, 3974–3975.

(13) See: Contant, R.; Thouvenot, R. *Inorg. Chim. Acta* **1993**, *212*, 41–50 and references cited therein.

(14) Coronado, E.; Müller, A.; Pope, M. In *Polyoxometalate Molecular Science*; Borras-Almenar, J. J., Eds.; Kluwer Academic Publishers: Dordrecht, The Netherlands, 2003.

(15) Zhang, J.; Bond, A. M. *Inorg. Chem.* **2004**, *43*, 8263–8271.

(16) (a) Contant, R. *Inorg. Synth.* **1990**, *27*, 104–111. (b) Comuzzi, C.; Dolcetti, G.; Trovarelli, A.; Cavani, F.; Trifirò, F.; Llorca, J.; Finke, R. G. *Catal. Lett.* **1996**, *36*, 75–79. (c) Kawafune, I.; Matsubayashi, G. *Bull. Chem. Soc. Jpn.* **1996**, *69*, 359–365.

(17) Anderson, T. M.; Hill, C. L. *Inorg. Chem.* **2002**, *47*, 4252–4258.

(18) (a) López, X.; Bo, C.; Poblet, J.-M. *Inorg. Chem.* **2003**, *42*, 2634–2638. (b) López, X.; Bo, C.; Poblet, J.-M. *J. Am. Chem. Soc.* **2002**, *124*, 12574–12582.

(19) Poblet, J. M.; Bo, C. *Chem. Soc. Rev.* **2003**, *32*, 297–308.

(20) (a) Jeannin, Y.; Margin-Frere, J. *Inorg. Chem.* **1979**, *18*, 3010–3014. (b) Ozawa, Y.; Sasaki, Y. *Chem. Lett.* **1987**, *185*, 923–926. (c) Krebs, B.; Droste, E.; Piepenbrink, M.; Vollmer, G. *C. R. Acad. Sci., Sér. IIc: Chim.* **2000**, *3*, 205–210. (d) Constant, R.; Piro-Sellem, S.; Canny, J.; Thouvenot, R. *C. R. Acad. Sci., Sér. IIc: Chim.* **2000**, *3*, 157–161. (e) Wang, J.-P.; Ma, P.-T.; Zhao, J.-W.; Niu, J.-Y. *Inorg. Chem. Commun.* **2007**, *10*, 523–526. (f) Long, D.-L.; Streb, C.; Song, Y.-F.; Mitchell, S.; Cronin, L. *J. Am. Chem. Soc.* **2008**, *130*, 1830–1832.

(21) (a) Long, D.-L.; Kögerler, P.; Cronin, L. *Angew. Chem., Int. Ed.* **2004**, *43*, 1817–1820. (b) Long, D.-L.; Abbas, H.; Kögerler, P.; Cronin, L. *Angew. Chem., Int. Ed.* **2005**, *44*, 3415–3419. (c) Baffert, C.; Boas, J. F.; Bond, A. M.; Kögerler, P.; Long, D.-L.; Cronin, L. *Chem.—Eur. J.* **2006**, *12*, 8472–8483. (d) Fay, N.; Bond, A. M.; Baffert, C.; Boas, J. F.; Pilbrow, J. R.; Long, D.-L.; Cronin, L. *Inorg. Chem.* **2007**, *9*, 3502–3510.

(22) (a) Long, D.-L.; Kögerler, P.; Parenty, A. D. C.; Fielden, J.; Cronin, L. *Angew. Chem., Int. Ed.* **2006**, *45*, 4798–4803. (b) Yan, J.; Long, D.-L.; Wilson, E. F.; Cronin, L. *Angew. Chem., Int. Ed.* **2009**, *48*, 4376–4380. (c) Long, D.-L.; Song, Y. F.; Wilson, E. F.; Kögerler, P.; Guo, S. X.; Bond, A. M.; Hargreaves, J. S. J.; Cronin, L. *Angew. Chem., Int. Ed.* **2008**, *47*, 4384–4387. (d) Long, D.-L.; Song, Y.-F.; Wilson, E.; Kögerler, P.; Guo, S.-X.; Bond, A. M.; Hargreaves, J. S. J.; Cronin, L. *Angew. Chem., Int. Ed.* **2008**, *120*, 4456–4459.

(23) Kortz, U.; Pope, M. T. *Inorg. Chem.* **1994**, *33*, 5643–5646.

(24) (a) Jorris, T. L.; Kozik, M.; Baker, J. C. W. *Inorg. Chem.* **1990**, *29*, 4584–4586. (b) Khenkin, A. M.; Neumann, R. *Inorg. Chem.* **2000**, *39*, 3455–3462.

(25) (a) Zhang, F.-Q.; Guan, W.; Zhang, Y.-T.; Xu, M.-T.; Li, J.; Su, Z.-M. *Inorg. Chem.* **2010**, *49*, 5472–5481. (b) Zhang, F.-Q.; Zhang, X.-M.; Wu, H.-S.; Hai, J. *J. Phys. Chem. A* **2007**, *111*, 159–166. (c) Zhang, F.-Q.; Zhang, X.-M.; Wu, H.-S.; Li, Y.-W.; Hai, J. *J. Phys. Chem. A* **2007**, *111*, 1683–1687. (d) Zhang, F.-Q.; Wu, H.-S.; Xu, Y.-Y.; Li, Y.-W.; Hai, J. *J. Mol. Model.* **2006**, *12*, 551–558. (e) Zhang, F.-Q.; Wu, H.-S.; Qin, X.-F.; Li, Y.-W.; Jiao, H. *J. Mol. Struct. (Theochem.)* **2005**, *755*, 113–117.

(26) Graham, C. R.; Finke, R. *Inorg. Chem.* **2008**, *47*, 3679–3686.

(27) Yan, L.; López, X.; Carbó, J. J.; Sniatynsky, R.; Duncan, D. C.; Poblet, J.-M. *J. Am. Chem. Soc.* **2008**, *130*, 8223–8233.

(28) (a) Delley, B. *J. Chem. Phys.* **1990**, *92*, 508–517. (b) Delley, B. *J. Chem. Phys.* **2000**, *113*, 7756–7764.

(29) (a) Keal, T. W.; Tozer, D. J. *J. Chem. Phys.* **2004**, *121*, 5654–5660. (b) Keal, T. W.; Tozer, D. J. *J. Chem. Phys.* **2003**, *119*, 3015–3024.

(30) (a) Chang, C.; Pelissier, M.; Durand, M. *Phys. Scr.* **1986**, *34*, 394–404. (b) van Lenthe, E.; Baerends, E. J.; Snijders, J. G. *J. Chem. Phys.* **1993**, *99*, 4597–4610. (c) van Lenthe, E.; Baerends, E. J.; Snijders, J. G. *J. Chem. Phys.* **1994**, *101*, 9783–9792. (d) van Lenthe, E.; Snijders, J. G.; Baerends, E. J. *J. Chem. Phys.* **1996**, *105*, 6505–6516. (e) van Lenthe, E.; van Leeuwen, R.; Baerends, E. J.; Snijders, J. G. *Int. J. Quantum Chem.* **1996**, *57*, 281–293. (f) van Lenthe, E.; Ehlers, A. E.; Baerends, E. J. *J. Chem. Phys.* **1999**, *110*, 8943–8953.

(31) (a) Klamt, A.; Schüümann, G. *J. Chem. Soc., Perkin Trans.* **1993**, *2*, 799–805. (b) Klamt, A. *J. Chem. Phys.* **1995**, *99*, 2224–2235.

(32) López, X.; Fernández, J. A.; Romo, S.; Paul, J. F.; Kanzansky, L.; Poblet, J.-M. *J. Comput. Chem.* **2004**, *25*, 1542–1549.

(33) (a) Hervé, G.; Tezé, A. *Inorg. Chem.* **1977**, *16*, 2115–2117. (b) Pope, M. T. *Inorg. Chem.* **1977**, *16*, 2008–2010.

(34) 3.333/3.678 Å (0.345) and 3.332/3.714 Å (0.382) in α and γ, respectively, and 3.346/3.677 Å (0.331) and 3.313/3.712 Å (0.399) in β, which consists of nonequivalent halves. The data in parenthesis are the calculated differences.

(35) No W_b-W_b differences were observed between α and α* or γ and γ^*, which are built of the two equivalent $\{PW_9\}$. Differences were only observed in β and β^*, i.e., 3.346/3.313 Å (0.033) and 3.677/3.712 Å (0.035).

(36) 3.409/3.660 Å (0.251) and 3.368/3.702 Å (0.334) in α* and γ^*, respectively, and 3.374/3.666 Å (0.292) and 3.396/3.689 Å (0.293) in β^*, which consists of nonequivalent halves.

(37) The same range for the W_b-W_b difference with the same belt. See Figure S1 in the Supporting Information for details.

(38) Average data of β_α (0.331 Å) > $\beta_\alpha{}^*$ (0.292 Å) and β_β (0.399 Å) > $\beta_\beta{}^*$ (0.293 Å) in β/β^* consist of nonequivalent halves, where the subscript denotes $\{XW_9\}$ types.

(39) Zhang, F.-Q.; Wu, H.-S.; Cao, D.-B.; Zhang, X.-M.; Li, Y.-W.; Jiao, H. *J. Mol. Struct. (Theochem.)* **2005**, *755*, 119–126.

(40) Maksimovskaya, R. I.; Maksimov, G. M.; Litvak, G. S. *Russ. Chem. Bull.* **2003**, *52*, 103–108.

(41) 11.1°, 21.8°/14.8°, and 3.4° for α*, β^*, and γ^*, respectively.

(42) Jansen, S. A.; Wang, S.-H.; Eddowes, A. D. *Supramol. Sci.* **1997**, *4*, 51–58.

(43) For staggered-belt structures including α*, β and γ^*, the distance between the two planes composed of the metal atoms is used.

(44) Average data of 7.025 and 7.023 Å of two nonequivalent halves in β structure.

(45) For staggered-belt structures including α*, β, and γ^*, the distance between the two planes composed of the terminal O atoms is used.

(46) Average data of 10.353 and 10.330 Å of nonequivalent halves in the β structure.

(47) 3.368, 3.361/3.363, and 3.373 Å for α, β, and γ, respectively.

(48) Average data of 3.358/3.409 Å in β^*.

(49) (a) Mayer, I. *Chem. Phys. Lett.* **1983**, *97*, 270–274. (b) Mayer, I. *Int. J. Quantum Chem.* **1984**, *26*, 151–154.

(50) Day, V. W.; Klemperer, W. G. *Science* **1985**, *228*, 533–541.

(51) (a) Bridgeman, A. J.; Cavigliasso, G. *J. Phys. Chem. A* **2001**, *105*, 7111–7117. (b) Bridgeman, A. J. *Chem.—Eur. J.* **2004**, *10*, 2935–2941.

(52) Evaluated by $|\Delta E_{free}|/(|\Delta FIE| + |\Delta E_{free}| + |\Delta DE|)$, where "$|\cdots|$" denotes the absolute value.

(53) Rohmer, M.-M.; Bénard, M.; Blaudeau, J.-P.; Maestre, J.-M.; Poblet, J.-M. *Coord. Chem. Rev.* **1998**, *178*−*180*, 1019–1049.
(54) Evaluated by $|\Delta FIE|/(|\Delta FIE| + |\Delta E_{free}| + |\Delta DE|)$, where "$|\cdots|$" denotes the absolute value.
(55) Axial 107.6°, 107.6°/107.9°, 107.8°, 107.7°, 107.6°/107.6°, and 107.7° and radial 111.2°, 111.3°/111.0°, 111.1°, 111.2°, 111.3°/111.3°, and 111.3° for α, *β*, *γ*, α*, *β**, and *γ**, respectively.
(56) López, X.; Maestre, J. M.; Bo, C.; Poblet, J.-M. *J. Am. Chem. Soc.* **2001**, *123*, 9571–9578.
(57) The O−H bond length of $O{=}W(OH)_4/C_{2v}$ was optimized at the KT2/TZP level, and it is very close to that (0.96 Å) of water.
(58) (a) Lau, T.-C.; Wang, J.; Guevremont, R.; Siu, K. W. M. *Chem. Commun.* **1995**, 877–878. (b) Huang, X.; Zhai, H.-J.; Kiran, B.; Wang, L.-S. *Angew. Chem., Int. Ed.* **2005**, *117*, 7417–7420.
(59) (a) Finke, R. G.; Droege, M. W.; Domaille, P. J. *Inorg. Chem.* **1987**, *26*, 3886. (b) Constant, R.; Ciabrini, J.-P. *J. Chem. Res., Synop.* **1977**, 222. (c) Fang, X.; Hill, C. L. *Angew. Chem., Int. Ed.* **2007**, *46*, 3877.
(60) Dumas, E.; Debiemme-Chouvy, C.; Sevov, S. C. *J. Am. Chem. Soc.* **2002**, *124*, 908–909.
(61) (a) Arendt, E.; McEvoy, K. M.; Gaigneaux, E. M. *Appl. Catal., A* **2009**, *357*, 115–124. (b) Hu, J.; Burns, R. C.; Guerbois, J.-P. *J. Mol. Catal. A: Chem.* **2000**, *152*, 141–155. (c) Comuzzi, C.; Dolcetti, G.; Trovarelli, A.; Cavani, F.; Trifirò, F.; Llorca, J.; Finke, R. G. *Catal. Lett.* **1996**, *36*, 75–79.
(62) (a) Schomaker, V.; Waser, J.; Marsh, R. E.; Bergman, G. *Acta Crystallogr.* **1959**, *12*, 600.(b) Scheringer, C. *Acta Crystallogr.* **1971**, *B27*, 1470−1472. The source code of the least-squares best-fit plane is obtained free of charge from http://www.bmm.icnet.uk/people/suhail/plane.html.
(63) Hybridization type of O in water with an angle H−O−H of 104.5°.
(64) 3.589/3.604 Å in $[W_9O_{30}]^{6-}/C_{3v}$ optimized in the gas phase.
(65) (a) Pope, M. T.; Papaconstantinou, E. *Inorg. Chem.* **1967**, *6*, 1147–1152. (b) Papaconstantinou, E.; Pope, E. *Inorg. Chem.* **1967**, *6*, 1152–1155. (c) Varga, G. M.; Papaconstantinou, E.; Pope, E. *Inorg. Chem.* **1970**, *9*, 662–667. (d) Papaconstantinou, E.; Pope, E. *Inorg. Chem.* **1970**, *9*, 667–669.
(66) Suaud, N.; Gaita-Ariño, A.; Clemente-Juan, J. M.; Sánchez-Marin, J.; Coronado, E. *J. Am. Chem. Soc.* **2002**, *124*, 15134–15140.
(67) Borrás-Almenar, J. J.; Clemente-Juan, J. M.; Coronado, E.; Tsukerblat, B. S. *Chem. Phys.* **1995**, *195*, 1–15.
(68) (a) Winget, P.; Weber, E. J.; Cramer, C. J.; Truhlar, D. G. *Phys. Chem. Chem. Phys.* **2000**, *2*, 1231–1239. (b) Baik, M.-H.; Silverman, J. S.; Yang, I. V.; Ropp, P. A.; Szalai, V. A.; Yang, W. T.; Thorp, H. H. *J. Phys. Chem. B* **2001**, *105*, 6437–6444. (c) Patterson, E. V.; Cramer, C. J.; Truhlar, D. G. *J. Am. Chem. Soc.* **2001**, *123*, 2025–2031. (d) Baik, M.-H.; Friesner, R. A. *J. Phys. Chem. A* **2002**, *106*, 7407–7412. (e) Arnold, W. A.; Winget, P.; Cramer, C. J. *Environ. Sci. Technol.* **2002**, *36*, 3536–3541. (f) Fu, Y.; Liu, L.; Yu, H. Z.; Wang, Y. M.; Guo, Q. X. *J. Am. Chem. Soc.* **2005**, *127*, 7227–7234. (g) Fu, Y.; Liu, L.; Wang, Y. M.; Li, J. N.; Yu, T. Q.; Guo, Q. X. *J. Phys. Chem. A* **2006**, *110*, 5874–5886.
(69) Fay, N.; Dempsey, E.; Kennedy, A.; McCormac, T. *J. Electroanal. Chem.* **2003**, *556*, 63–74.
(70) (a) Chiang, M.-H.; Antonio, M. R.; Soderholm, L. *Dalton Trans.* **2004**, 3562–3567. (b) Himeno, S.; Takamoto, M.; Santo, A.; Ichimura, A. *Bull. Chem. Soc. Jpn.* **2005**, *78*, 95–100.
(71) López, X.; Fernández, J.; Poblet, J. M. *Dalton Trans.* **2006**, 1162–1167.
(72) (a) Mbomekallé, I.-M.; López, X.; Poblet, J. M.; Sécheresse, F.; Keita, B.; Nadjo, L. *Inorg. Chem.* **2010**, *49*, 7001–7006. (b) Fernández, J. A.; López, X.; Bo, C.; de Graaf, C.; Baerends, E. J.; Poblet, J. M. *J. Am. Chem. Soc.* **2007**, *129*, 12244–12253.
(73) Computed as E_{LUMO}(anion) − E_{LUMO}(host cage), i.e., 2.273/α, 2.274/*β*, 2.264/*γ*, 2.270/α*, 2.262/*β**, and 2.265/*γ** eV, respectively.
(74) (a) Tourné, C.; Revel, A.; Tourné, G. *Rev. Chim. Miner.* **1977**, *14*, 537–542. (b) Fuchs, J.; Palm, R. *Z. Naturforsch., B* **1984**, *39*, 757–761. (c) Contant, R. *Can. J. Chem.* **1987**, *65*, 568–573.
(75) For example, see: (a) Laclerc-Laronze, N.; Marrot, J.; Hervé, G. *Inorg. Chem.* **2005**, *44*, 1275–1281. (b) Laronze, N.; Marrot, J.; Hervé, G. *Inorg. Chem.* **2003**, *42*, 5857–5862. (c) Sun, C.-Y.; Liu, S.-X.; Wang, C.-L.; Xie, L.-H.; Zhang, C.-D.; Gao, B.; Su, Z.-M.; Jia, H.-Q. *J. Mol. Struct.* **2006**, *785*, 170–175.
(76) (a) Ziegler, T.; Rauk, A. *Inorg. Chem.* **1979**, *18*, 1558–11565. (b) Ziegler, T.; Rauk, A. *Inorg. Chem.* **1979**, *18*, 1755–1759. (c) Ziegler, T.; Rauk, A. *Theor. Chim. Acta* **1977**, *46*, 1–10.
(77) Albright, T. A.; Burdett, J. K.; Whangbo, M.-H. *Orbital Interactions in Chemistry*; Wiley: New York, 1985.
(78) (a) Landrum, G. A.; Goldberg, N.; Hoffmann, R. *J. Chem. Soc., Dalton Trans.* **1997**, 3605–3613. (b) Bickelhaupt, F. M.; Baerends, E. J. *Rev. Comput. Chem.* **2000**, *15*, 1–86.